STEP-AND-SCAN AND STEP-AND-REPEAT, A TECHNOLOGY COMPARISON

Martin van den Brink, Hans Jasper, Steve Slonaker, Peter Wijnhoven and Frans Klaassen

ASM Lithography
De Run 1110
5503 LA Veldhoven
The Netherlands

This paper was first presented at the
SPIE Symposium on Microlithography,
Santa Clara, March 10-15, 1996.

STEP-AND-SCAN AND STEP-AND-REPEAT, A TECHNOLOGY COMPARISON

Martin van den Brink, Hans Jasper, Steve Slonaker, Peter Wijnhoven and Frans Klaassen
ASM Lithography, De Run 1110, 5503 LA Veldhoven, The Netherlands

ABSTRACT

While the semiconductor manufacturing community is preparing for the transition from 0.35 μm to 0.25 μm technology, lithography equipment suppliers are preparing for the shift from step-and-repeat to step-and-scan systems.

In addition, most wafer stepper users are planning to change from i-line to KrF laser wavelength technology. The question, however, is what are the advantages and disadvantages of scanners over steppers in a production environment. In this paper, we discuss the two different technologies using the following criteria:

1. Throughput/cost of ownership,
2. CD control/depth of focus,
3. Distortion and overlay.

248 nm lithography will be used for the 0.25 μm process rule regime in combination with i-line systems being used for 50 to 70% of the lithography steps (exposing the non-critical layers) to reduce cost. Therefore, an ideal match is required between i-line systems and their DUV critical layer counterparts.

For this reason, the economic equation of step-and-scan is determined by the total picture of matched DUV and i-line scanners. However, the comparisons between non-laser-based scanners and steppers and laser-based scanners and steppers are different. This paper discusses this subject using a combination of theoretical modelling and measured data. Imaging data from a new, DUV, double telecentric, 0.4 to 0.57 variable NA wafer stepper equipped with a variable coherence/annular illuminator is shown; thus proving that good imaging data at 0.25 μm resolution at moderate cost is possible using wafer steppers.

Also, the performance data of a step-and-scan system, currently in development, is given, thus showing that high performance and high throughput scanners can be built. From this, it will be shown that the choice between steppers and scanners depends upon the combination of design rules, cost of ownership and required chip size.

1. STEP-AND-SCAN VERSUS STEP-AND-REPEAT — AN INTRODUCTION TO THE TECHNOLOGY AND THE COMPARISON METHOD

The lithography requirements for wafer steppers can be derived from the SIA road map, which is summarised in Table 1 [1]. As indicated, field size increases by 50% every six years and resolution is halved every six years. This means that the number of pixels to be imaged during one exposure triples every six years. Lens production cost is approximately proportional to the number of pixels imaged, as shown in Figure 1 [2] [3].

The increase in lens cost is mainly driven by the following factors:

- There is an increase in the glass volume required.
- It is more difficult to reach refractive index uniformity over a larger glass diameter, including the associated metrology.
- Due to the lower resolution, tighter aberration control of the lens, including associated metrology issues, is required.

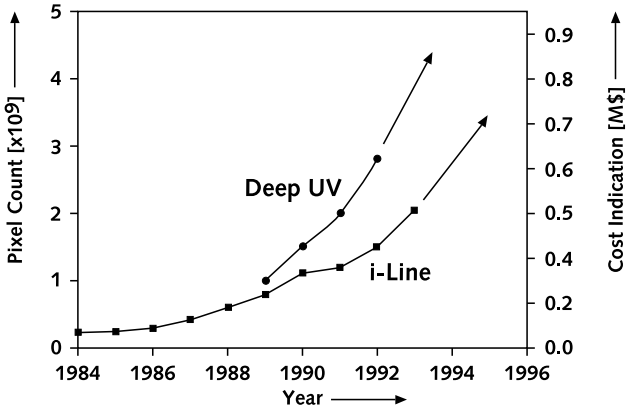

Figure 1 Pixel count and cost of lithographic lenses

- Tighter surface accuracy, including the associated metrology issues, are required.
- Larger glass diameters make mounting, to accommodate the thermal expansion differences combined with low mounting stress requirements, more difficult.
- Coating requirements are more difficult due to larger

Table 1 Critical level lithography requirement according to the SIA [1]

Year of first shipment	1995	1998	2001	2004	2007	2010
Feature size [μm]	0.35	0.25	0.18	0.13	0.10	0.07
Bits (DRAM)	64 M	256 M	1 G	4 G	16 G	64 G
Overlay [nm]	100	75	50	40	40	20
Chip size [mm x mm]						
Logic	16 x 16	18 x 18	19 x 19	21 x 21	23 x 23	25 x 25
DRAM	10 x 20	12 x 24	15 x 30	18 x 36	22 x 44	28 x 50
CD uniformity [nm]	35	25	18	13	10	7
Defect density [m^{-2}]	690	320	135	TBD	TBD	TBD
Depth of focus [μm]	1.0	0.8	0.7	TBD	TBD	TBD
Resist thickness [μm]	1.22	0.87	0.63	Advanced systems		

diameters and lens apertures, resulting in a higher angular light distribution on the coatings.

To moderate the increase in cost, alternative exposure strategies need to be considered, as proposed by Markle in 1984 [4]. This lead to several lithography vendors using reduction lenses [5] [6]. Figure 2 shows a lens scan strategy where the exposure on the scanner can be released with a lens image field surface up to five times smaller than required on the stepper, assuming a 1:2 aspect ratio and a small scan slit.

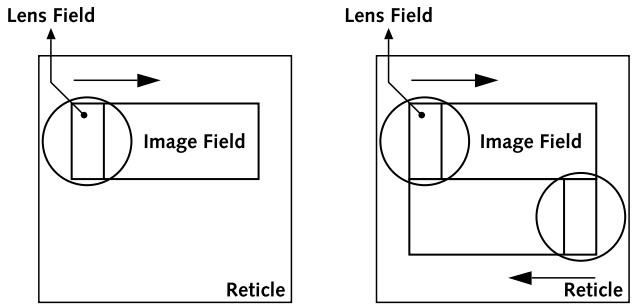

Figure 2 Single pass and double pass step-and-scan

For a 1:1 aspect ratio, the image field surface gain is up to a factor of two. This benefit can directly be translated into a lens cost saving by the same factor. If the throughput of both systems is the same, it is easy to understand that the savings easily compensate for the additional costs of the scanning function. With refractive lenses, the system architecture can be highly compatible with the wafer stepper architecture currently in use. This means that there are only moderate cost differences between stepper and scanner bodies. Figure 3 shows a typical step-and-scan architecture.

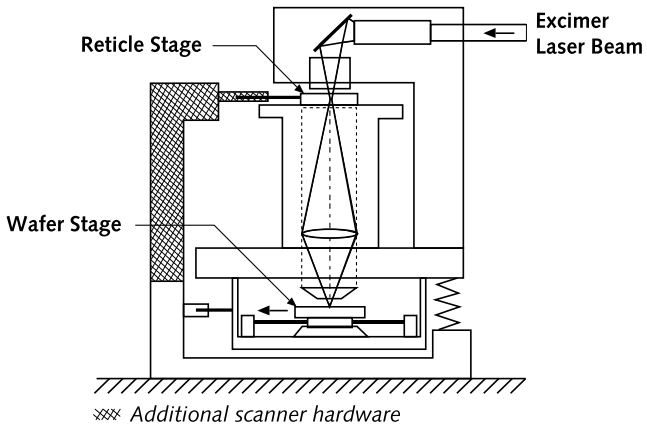

Figure 3 Scanning wafer stepper

The major difference between a stepper and a scanner is the scanning stage at reticle level. As also shown in Figure 2, by scanning and stitching at the same time, similarly to the earlier proposal [4], the field size can be extended to whatever size is needed without increasing the lens field size and, at the same time, reducing the distortion and the CD butting errors (which occur with stepper field stitching).

If the above argument was complete, we could conclude that scanners are the ideal solution. However, the performance of steppers and scanners is not determined by system cost only. The following factors should also be taken into account when comparing the two technologies:

- Throughput/cost of ownership,
- CD control/depth of focus,
- Distortion/overlay.

Since, for 0.25 μm rules, a mixture of UV and DUV tools will be used, the above questions need to be evaluated for both technologies. The logic of the comparison is as follows:

- In Section 2, we focus on the economic merits of steppers and scanners. This comparison is made independently for DUV and UV because these technologies have different economic driving factors. A more thorough discussion of the various economic equations is included in the appendices.
- Section 3 is focused on the difference in the imaging performance of steppers and scanners. With limited scanner system statistics available, we have used measured performance data of ten i-line systems as well as wafer flatness measurements of 20 wafers. Data on stage synchronisation of our step-and-scan prototype is shown and used to determine the impact of stage synchronisation on image degradation. All data is used to simulate the image performance of scanners and steppers. The simulator is described in an appendix.
- From the above, it is concluded, in Section 4, that if the product design calls for a field size of 22 x 22 mm and a feature size of 0.25 μm, the imaging advantages of scanning systems do not seem to be strong enough to compensate for the economic penalty. This may mean that scanners are expected to be used where field sizes, larger than 22 x 22 mm, and/or imaging 0.20 μm features and below are required.
- Finally, experimental data of a new DUV stepper model is shown in Section 5; illustrating that good imaging at 0.25 μm can be achieved using a stepper at moderate system cost

2. STEP-AND-SCAN VERSUS STEP-AND-REPEAT — AN ECONOMIC COMPARISON

2.1. General step-and-scan throughput considerations

To make a true comparison between steppers and scanners in terms of throughput and cost of ownership, it is necessary to assume equal capabilities for die size, stepping time, alignment time, wafer handling time etc. Having made these assumptions, the throughput differences between steppers and scanners are mainly related to the exposure time and exposure field size. This also assumes that the reticle and wafer stage performance parameters are designed such that the scan speed acceleration and de-acceleration can be done in parallel with the step time of the wafer in the non-scanned direction.

Figure 4 shows one of the fundamental differences between the exposure times of scanners and steppers. This difference is known as overscan.

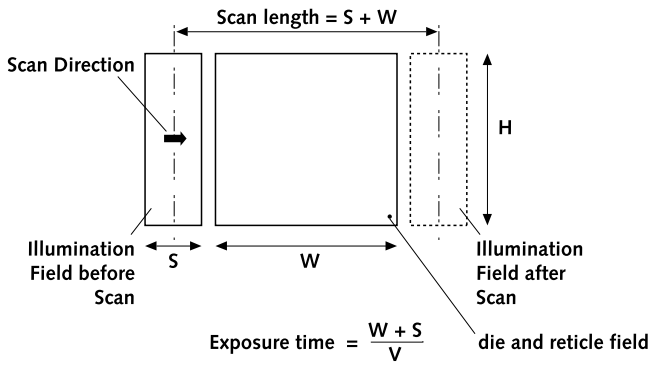

Figure 4 The die needs to move in and out of the scanning field; overscan per die

Overscan means that the mask needs to be scanned in and out of the illuminated scan slit. In doing this, the fundamental difference between the scanner and stepper exposure time is equal to the scan slit divided by the scan speed. The scanner exposure time is given by:

$$T_{ss} = \frac{W + S}{V} \quad (1)$$

Where:

T_{ss}	: Step-and-scan exposure time	[s]
W	: Die width	[mm]
S	: Slit width	[mm]
V	: Scan speed	[mm/s]

At a scan speed of 100 mm/s and a scan slit of 10 mm, the overscan time will take 100 ms. For a die length of 30 mm, this effect is about 30% of the total exposure time. While the reticle is being scanned in and out of the exposure field, illumination power is wasted outside the patterned reticle field. This leads to longer exposure times. This effect can partially be eliminated when the reticle pattern is extended with part of the next die, as shown in Figure 5.

Here, the start of the first exposed die is done in the normal way but the scan is now extended into the next die over the length of the slit width. The wafer stage steps to the start of the third die and scans back to the start of the second die. Then, the wafer stage moves back to the start of the third die and scans into the fourth die and so on. During the exposure of the last die in the row, the stage will be scanning out of the die or row. In this way, the wasted overscan time per die is reduced by the average row length. By exposing 20 x 20 mm dies on eight inch

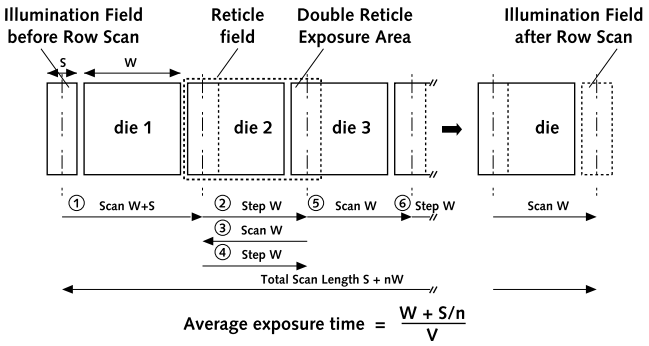

Figure 5 The row of dies needs to move in and out of the scanning field; overscan per row

wafers, this factor is about eight. Offsetting the throughput advantage is the larger required mask pattern, difficult reticle masking in the scan direction and a more complex dose control algorithm since the exposure of each die is composed of two separate scans.

Another factor is the limitation given by the stage technology. For a given stage technology in combination with a required accuracy, the stage scan speed is limited to a maximum V_m. The scan speed is determined by the dose as follows:

$$V = \frac{I_{ss} \cdot S}{D} \qquad (2)$$

Where:

I_{ss} : Slit intensity [mW/cm^2]
D : Dose [mJ/cm^2]

There is a lower dose limit. Below this limit, the exposure time does not decrease with the decreasing dose. The scan speed then determines the exposure time and the illumination power needs to be attenuated to maintain the relationship in (2). The effect of this phenomenon is given in Figure 6 for DUV scanners. In the

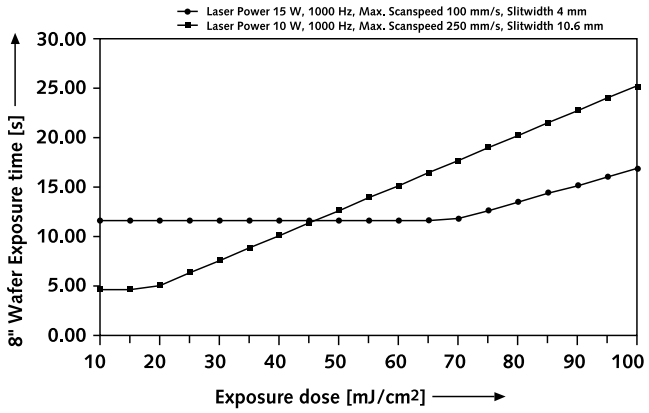

Figure 6 Total eight inch wafer exposure time of DUV scanners as function of exposure dose at different maximum scan speeds and laser power

figure, it is shown that a high power/low speed scanner is only competitive with a low power/high speed scanner above a certain minimum dose. If this dose is higher than the utilised resist dose sensitivity, the advantage of the high power is lost and the throughput is determined by the stage speed.

2.2. Pulsed laser source scanner analysis

Using pulsed laser sources, two main characteristics are important to our analysis.

1. Laser sources have a high brightness (see Appendix 1). This means that all of the energy of the laser can be shaped so that it will pass through the optical system. This allows the scanner slit to be minimised to improve the exposure time without reducing the total transmitted laser power.
2. A minimum number of pulses are required to realise an accurate energy dose distribution on the wafer. This minimum is determined by the dose control technology being used and is one of the more important discriminating scanner technologies (see Appendix 3).

The minimum number of pulses to make the dose and the minimum slit width to minimise the exposure time lead to a maximum possible scan speed determined by the dose requirement:

$$V < S \cdot \frac{f}{n} \qquad (3)$$

Where:

n : Minimum number of pulses to make the dose
f : Laser frequency [Hz]

The minimum number of pulses for an exposure is determined by the dose control technology of the stepper, illuminator and the laser. The dose quantisation effects of pulsed lasers sources in steppers and scanners have been published earlier [7]. The maximum frequency of the pulses is determined by the gas dynamics in the laser cavity and the maximum scan speed is limited by the stage technology. Therefore, the only parameter that can be freely chosen is the slit width. Thus, the optimum slit width is coupled to matching the stage, laser, illuminator and stepper technology by:

$$S = V_m \cdot \frac{n}{f} \qquad (4)$$

Where:

V_m : Maximum wafer stage speed [mm/s]

For example, at a stage speed of 250 mm/s, a minimum number of pulses of 32 and a laser frequency of 1000 Hz, the optimum slit width is 8 mm.

The effects, summarised in Equation (1) to Equation (4) inclusive, are shown in Figure 7, where the relative stepper to scanner exposure time (see Appendix 2) is given as function of slit width.

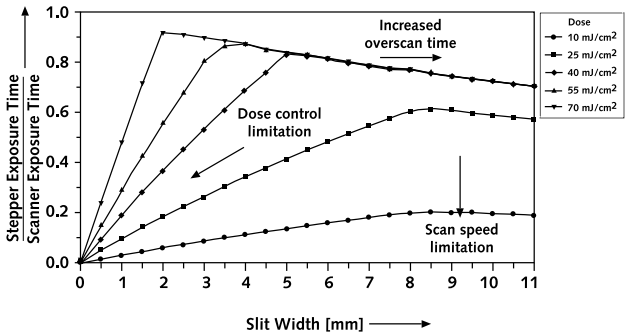

Figure 7 Relative DUV step-and-repeat and step-and-scan exposure time versus slit width at different exposure doses, 26 x 26 mm exposure fields, 10 W, 1000 Hz laser, 250 mm/s maximum scan speed

To make the comparison more direct, the stepper exposure time is divided by a scanner exposure time for equal field sizes. If this quotient is equal to 1, steppers and scanners have equal exposure times; if the quotient is less than 1, steppers are faster than scanners. For very small slit widths, the scanner dose accuracy requirement cannot be met. The scanner exposure time becomes dramatically longer than that of the stepper because the illumination power has to be attenuated. This comparison improves favourably, for the scanner, with increasing slit width. At a particular slit width, the dose accuracy requirement can easily be met. As the slit width increases further, the scanner again becomes slower than the stepper because of the increasing overscan time, as discussed above. The precise optimum is strongly related to the energy dose used. For low energy doses, the maximum scan speed is attained by increasing the slit width; the laser power remains attenuated and this leads to an exposure time that is unattractive when compared to steppers. Figure 8 shows the comparison of a 22 x 22 mm stepper and a 26 x 34 mm scanner as function of die size.

The measure, here, is the lithographic production capacity cost, which is the system cost times the wafer process time. The graph shows many minima and maxima determined by the change in the number of dies that fit in the exposure field. If the stepper field is fully utilised, this system is more cost effective. However, if the field is not utilised, the scanner would be more cost effective. At a die size of 22 x 22 mm, steppers are about 20% more competitive than scanners.

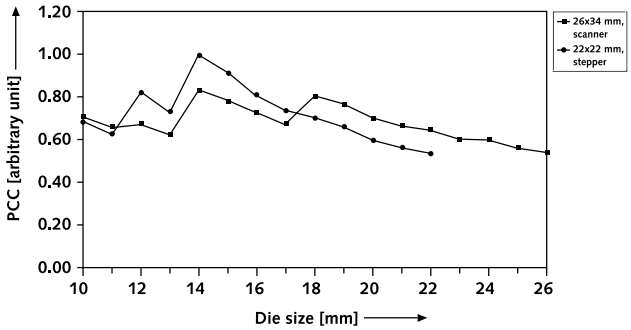

Figure 8 Production capacity cost of DUV steppers and scanners as a function of die size with 1:1 aspect ratio, 10.6 mm slit width, 250 mm maximum scan speed, 50 mJ/cm^2 dose, 10 W, 1000 Hz laser

2.3. Mercury lamp scanner analysis

Mercury lamp systems are continuous light sources, not hampered by the dose control problems of pulsed laser sources. It is, however, necessary to take measures to minimise dose variation due to lamp intensity variations. The largest problem of mercury lamp scanners is the combination of the desired small slit width and obtaining sufficient illumination power at the wafer. Due to the limited brightness of mercury lamps, as shown in Appendix 1, the smaller the slit the less power is transmitted through the lens. In fact, if mercury lamps with sufficient power can be manufactured, the lamp will always overfill the optical system and the larger the slit width, the shorter the exposure time (see Appendix 2). More generally, the minimum total exposure time that can be achieved by a projection system is determined by the optical throughput of the system (the optical throughput is equal to the product of field size and illumination angle). This means, for example, that larger wafer sizes will increase the total exposure time linearly with the exposed wafer surface area if the optical projection system remains the same [8]. This phenomenon is shown in Figure 9, where the relative exposure time of an i-line scanner with respect to an i-line stepper is shown as a function of slit width.

In contrast to Figure 7, which shows that DUV scanners can, by optimum scanner design, compete with steppers in terms of exposure times, i-line scanners suffer from competitive exposure times. The exposure times of I-line scanners are about double those of steppers. For a small slit width, the scanner exposure time is limited by the optical throughput of the scanner for all dose values. For low exposure doses, the scanner is stage speed limited, similarly to the above description. By increasing the slit width at low doses, the exposure time increases because of the longer overscan time. For high doses, the scanner

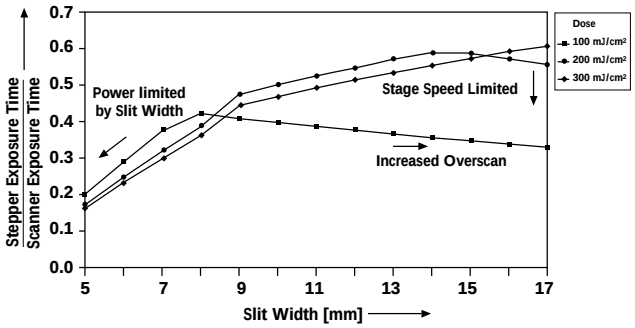

Figure 9 Relative i-line step-and-repeat/step-and-scan exposure time versus slit width at different exposure doses, 26 x 26 mm exposure fields, 2.5 kW mercury lamp, NA = 0.6, σ = 0.8, maximum scan speed = 250 mm/s

is limited by the optical throughput and the exposure time decreases continuously with increasing slit width. Thus, the main reason for the unpopularity of the mercury lamp scanner is throughput. Compared to steppers, the large slit required results in longer exposure times without a major reduction in lens complexity. It is expected that excimer lasers are the only source for DUV lithography because of the available power at the given bandwidth. For i-line, mercury lamps can be used to remain compatible with currently used lithography systems. To analyse the competitiveness of i-line scanners, it is necessary to bring the complete machine economics into consideration (see Appendix 4). A useful unit to determine this is, again, the lithographic production capacity cost, which is the machine cost multiplied by the wafer process time. At a small slit width, no illumination power will be transmitted through the optical system and the wafer process time will be very large, resulting in a high capacity cost. A large slit will lower the wafer process time but increase the lens cost, also resulting in a high capacity cost. This dependency is shown in Figure 10.

As shown, the minimum is relatively flat because increasing the throughput by selecting a larger slit will immediately be offset by a higher lens cost. The minimum is also dependent on the coherence value setting of the illuminator. At a coherence value of 0.8, the optimum slit width is close to 10 mm. For a coherence value of 0.3, the optimum slit width is close to 20 mm. Similar effects show up using off-axis illumination modes, which are, in general, limiting the optical throughput of the system.

A scanner with a slit width between 10 and 20 mm and a die height of 26 mm will have a lower throughput than a stepper but still an acceptable capacity cost because of the lower lens cost.

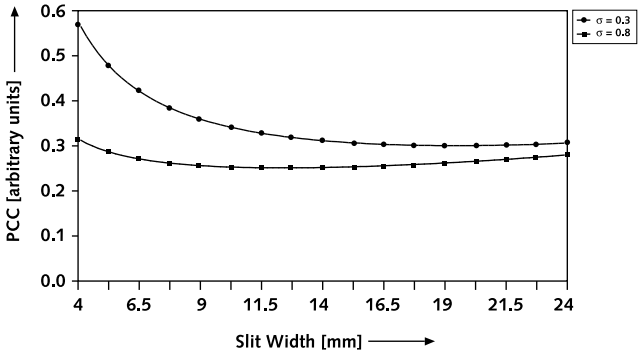

Figure 10 Production capacity cost of a mercury lamp scanner versus slit width at various doses and at different coherence values, 26 x 26 mm exposure fields, 2.5 kW mercury lamp, NA = 0.6, dose = 200 mJ/cm^2

Figure 11 shows the production capacity cost of a 26 x 34 mm scanner and a 22 x 22 mm stepper as a function of die size.

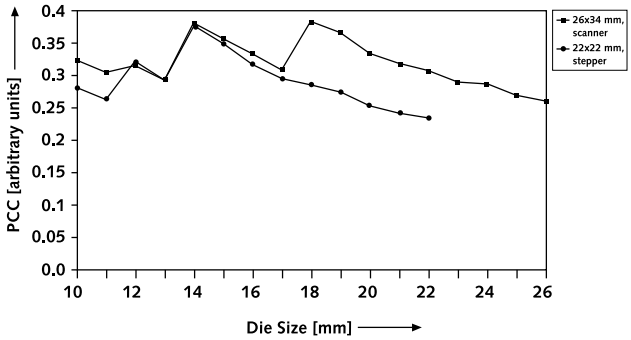

Figure 11 Production capacity cost of i-line steppers and scanners as function of die size, with 1:1 aspect ratio, 200 mJ/cm^2 exposure dose, 17 mm slit width

As shown, the i-line stepper is, from an economic point of view, a more attractive solution than a scanner and the use of scanners will be reserved for exposing larger field sizes in mix-and-match mode with the DUV counterpart.

Exposing 22 x 22 mm dies, the stepper is, as measured by the production capacity cost, about 30% more competitive than scanners. Assuming a mix of 30% DUV systems with 70% i-line systems in a production environment, scanners are about 27% more expensive to use than steppers. This number is, of course, sensitive to a number of parameters such as: scanner design, stepper design, die size etc.

3. STEP AND SCAN VERSUS STEP AND REPEAT, IMAGING PERFORMANCE

3.1. Analysis method

This section estimates the imaging quality performance difference between steppers and scanners. We use production data from ten PAS 5500/100 i-line steppers as a reference representing the current stepper performance. This stepper, with a numerical aperture of 0.6 and a field size of 22 x 22 mm, is evaluated both for distortion and field flatness over the whole field. From this imaging field data, a slit of 8 x 22 mm was selected and, in a simulator, scanned such that the aberrations were averaged over the slit width. Furthermore, stage synchronisation data of our step-and-scan prototype is used to estimate the impact of stage errors on the imaging performance. The simulator used is described in Appendix 5.

3.2. Scanning stage synchronization performance

The stage synchronization was tested in a step-and-scan prototype equipped with a 0.6 NA 22 x 22 mm i-line lens. Stage synchronization has been tested two ways, by just taking the error signal of the interferometer data and by making a so-called stage overlay. Figure 12a shows the stage interferometer error plot during the scan at a speed of 240 mm/s over a length of 40 mm.

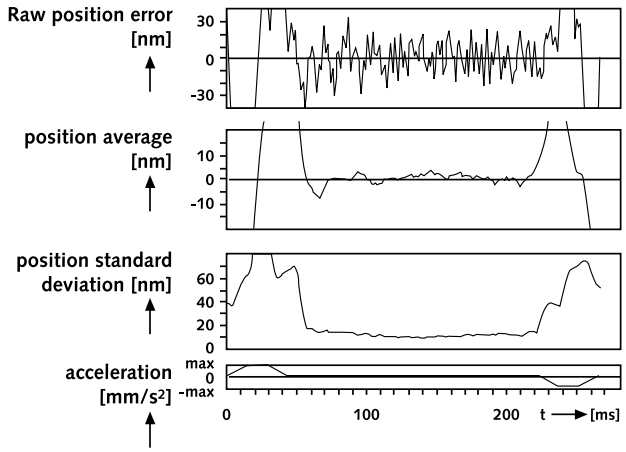

Figure 12 Wafer to reticle stage interferometer synchronization error measured at 240 mm/s with an 8 mm slit width

Figure 12b shows the average error measured over a moving slit of 8 mm. This represents the real stage error in an exposure. The value is measured below 5 nm, which is well below the overlay budget values for 0.18 μm lithography. Figure 12c shows the standard deviation of the stage vibration within a moving slit of 8 mm. This standard deviation can be translated into image contrast loss (see Appendix 5). A standard deviation of 15 nm, by imaging 0.25 μm lines and spaces, results in a contrast loss of 1.7%. Figure 12d shows the acceleration profile of the two stages showing that the settling time is virtually zero after the acceleration is set at zero. At a scan speed of 240 mm/s and a slit width of 8 mm it takes 33 ms before the average and standard deviation of the position can be determined.

Figure 13 shows a dynamic stage overlay measured at a speed of 100 mm/s, where two, nearly overlapping, exposures next to each other are made without taking the wafer out of the scanner between the exposures.

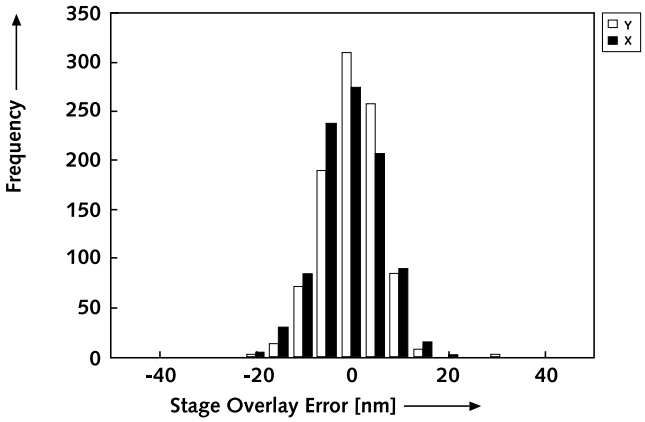

Figure 13 Stage overlay measurement exposed at 100 mm/s, 8 fields, 121 points per field, 8 mm slit width, 22 x 22 mm field, i-line lens

All correctable errors are removed from the data so that only non-systematic error components are shown. All measurements taken are below 20 nm.

3.3. Distortion

Figure 14a shows a distortion plot of a standard, currently-produced i-line lens using the system alignment system for the measurements.

As has been shown, the distortion contains a random component over the whole 22 x 22 mm field of up to 43 nm. In the same figure, the size of the scanning slit of 8.64 x 22 mm is given in which the distortion is reduced to 29 nm. This is because, in smaller field sizes, smaller distortion values can be more easily achieved. If this scan slit is scanned in the X direction over the 22 x 22 mm field (see Appendix 5), we would get the distortion pattern, as given in Figure 14b, where the maximum distortion is found to be 23 nm.

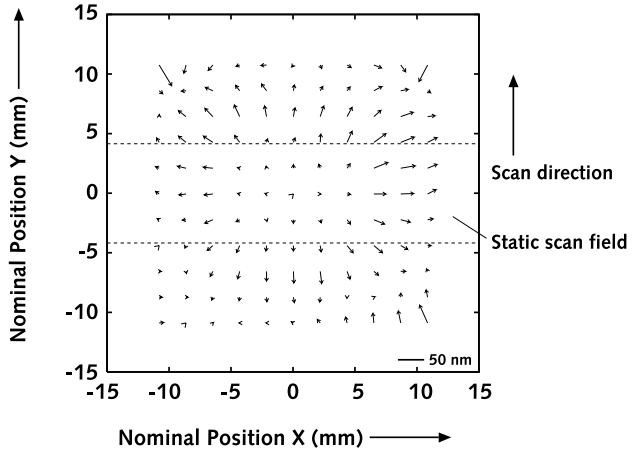

Figure 14a Distortion plot of a stepper and a scanner scanning the same 22 x 22 mm field size using the same lens measuring 121 points: measured stepper field, maximum stepper field distortion 43 nm, indicating a maximum distortion of 29 nm over the 8.64 mm static scanner field

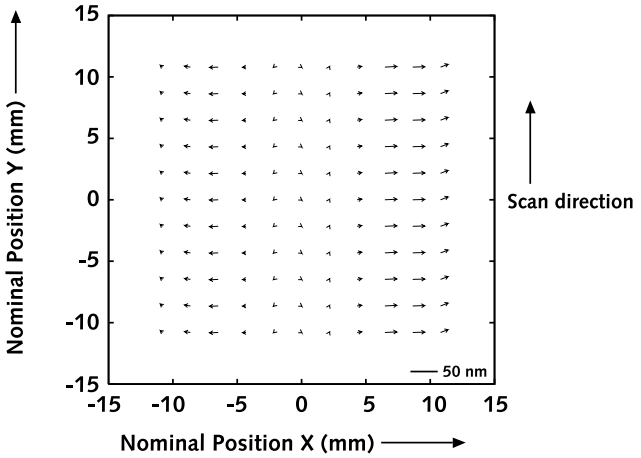

Figure 14b Distortion plot of a stepper and a scanner scanning the same 22 x 22 mm field size using the same lens measuring 121 points: simulated scanner field, maximum distortion 23 nm

Typically, for a scanner, the distortion pattern shows no variation in the scanned direction. Figure 15 shows the results of ten lenses measured in stepper mode and simulated in scanner mode.

As shown, the distortion values are reduced by a factor of two from an average of 39 nm for the stepper to 18 nm for the scanner. Referring to a previously published distortion analysis [9], the number of correctable distortion components in a scanner is larger than in a stepper. This can be shown by integrating the distortion model over the slit width (see also Appendix 5). Doing this, all uneven distortion terms are eliminated in the scanned direction. The stepper-correctable distortions are

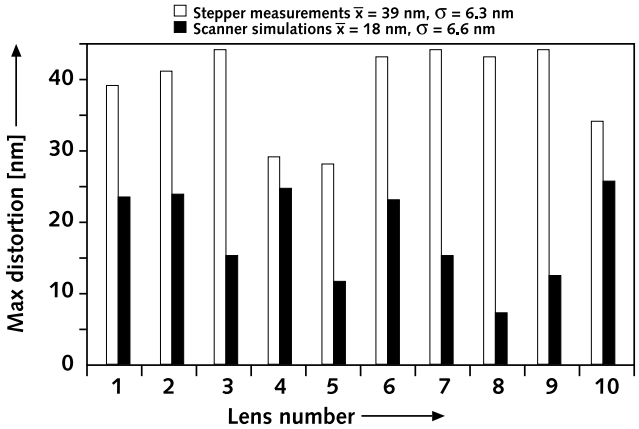

Figure 15 Maximum distortion measurement / simulation from ten lenses in stepper mode (22 x 22 mm) and scanner mode (22 x 8.64 mm)

translation, trapezoid, magnification and rotation. On a scanner we have to separate distortion in the scanned and non-scanned directions. In the scanned direction, rotation, trapezoid, third and fifth order distortions are eliminated. In the non-scanned direction, wedge distortion is eliminated. This means anamorphism and asymmetrical distortion components can be eliminated. For small slit widths, the third order distortion is reduce by 50% and the fifth order is reduced by 25% compared to a stepper field. Furthermore, there is no position dependency of the distortion pattern in the scanned direction, enabling smooth image stitching across edges perpendicular to the scanned direction.

3.4. Field and wafer flatness

Evaluating field flatness of the same lens set in stepper and scanner mode, we get similar plots as shown above. Figure 16 shows the values of the focal plane deviation measured on ten i-line lenses using the stepper alignment system for focus measurements [10].

Selecting a slit of 8.64 mm for each of the ten lenses and executing a simulated scan (see Appendix 5), the effective scanner focal plane deviation can be calculated. This reduces the average focal plane deviation from 288 nm on the stepper fields to 185 nm; an improvement of about 36%. The lenses used for the simulation are optimized to be used in a stepper. If the aberrations need only to be optimized in the scan field, even more reduction can be expected for both distortion and focal plane deviation. Figure 17 shows the focal plane deviation distribution of the measured stepper fields and the simulated scanner fields. In this figure, all measured 121 data points per lens are shown, in contrast with Figure 16, where the maximum field flatness values per

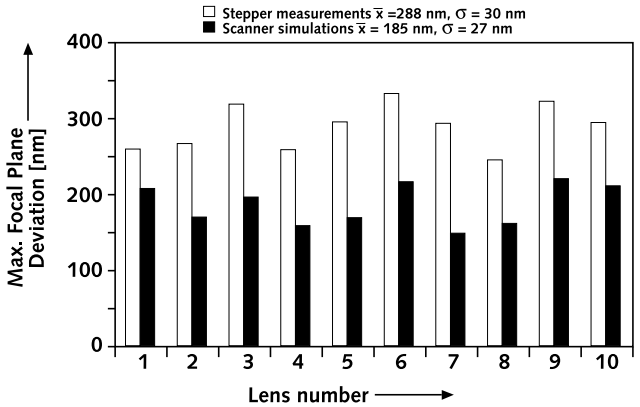

Figure 16 Maximum focal plane deviation of ten i-line stepper lenses measured over 22 x 22 mm and corresponding simulated data in scanning mode selecting a 22 x 8.64 mm static scan field

lens are shown. The distribution width of the scanner is about 14% less than that of the stepper.

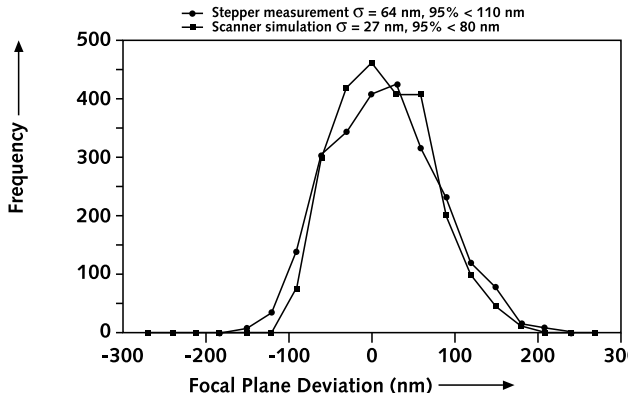

Figure 17 Focal plane deviation measurement/simulation distribution of ten i-line lenses in stepper mode (22 x 22 mm) and scanner mode (22 x 8.64 mm) measuring 121 points per lens

In addition to focal plane deviation, we also expect differences in wafer unflatness. Twenty "flat" wafers are measured using the stepper focus system. The unflatness is evaluated over 22 x 22 mm, using nine points of the stepper field, and 22 x 8 mm, using nine points of a scanner field. This assumes that, during the scan operation, the scanner focus system continuously and actively focuses the scanning field of 22 x 8 mm to the wafer.

The results are given in Figure 18, where the standard deviation of the wafer flatness distribution for steppers, 142 nm, reduces by about 45% for scanners, to 78 nm.

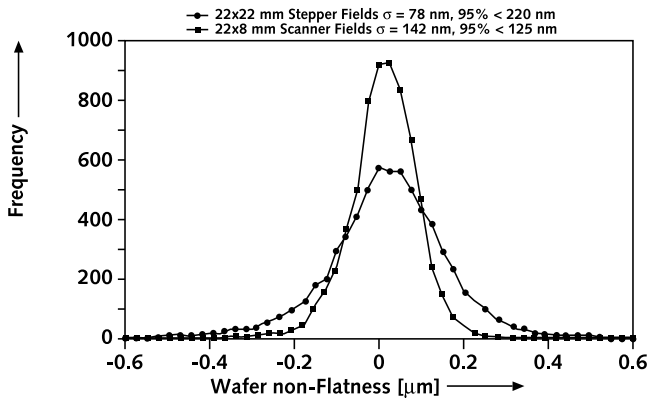

Figure 18 Wafer non flatness distribution of 20 eight inch wafers, 37 dies, 9 points per die, 6660 data points

3.5. Focus exposure window

With all these imaging advantages of scanners over steppers, it is possible to quantify the total effect in terms of the focus exposure window difference. With the above distortion and focus measurement simulation, a comparative error budget for steppers and scanners can be developed, as shown in Table 2, whose values are based on the above measurements and simulations.

Table 2 Comparative stepper/scanner error budget

Focus/position variation	Steppers	Scanners
Focus variation		
Wafer non-flatness	142	78
Focal plane deviation	62	55
Focus sensor	50	50
Scanning Z-accuracy	-	40
Total focus variation (RMS)	163	115
Position averaging		
Distortion averaging	-	4
Scan noise	-	15
Total position variation (RMS)	-	16

Translating these component image disturbances into a general image disturbance was published earlier [11] and we use a similar calculation method, as described in Appendix 5. Both distortion and field flatness averaging lead to smaller distortion and field flatness values but result also in a degree of contrast loss. Assuming a sinusoidal image contrast of 0.25 μm lines and spaces, 15 nm position vibration leads to 1.7% contrast loss and

100 nm focus vibration leads to 1.6% contrast loss. Both effects need to be taken into account to calculate the total difference between stepper and scanner imaging. Table 2 is now being used as input to simulate the focus exposure combination of 0.25 μm and 0.20 μm lines and spaces at 10% CD variation. The result is shown in Figure 19a and Figure 19b.

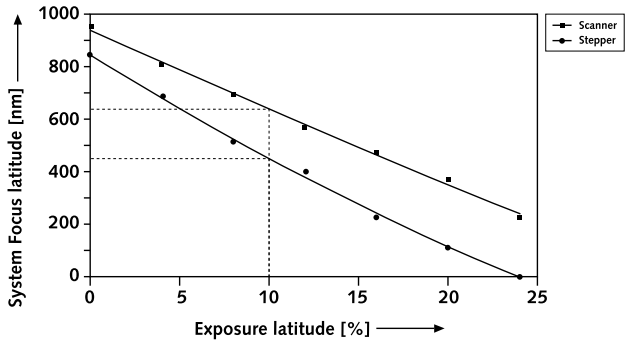

Figure 19a Comparative stepper / scanner system focus exposure window for 0.25 μm lines and spaces at 10% CD variation using a 0.57 NA DUV lens (data includes field and wafer flatness)

Figure 19a shows the exposure system defocus curve simulated for 0.25 μm. At 10% energy tolerance, the system depth of focus of the stepper (0.45 μm) is about 27% less than for the scanner (0.62 μm). This system depth of focus calculation is now completely available for the process and includes all the parameters summarised in Table 2, in contrast to lens depth of focus, where only lens parameters are taken into consideration. Figure 19b shows the same simulation for 0.20 μm lines and spaces.

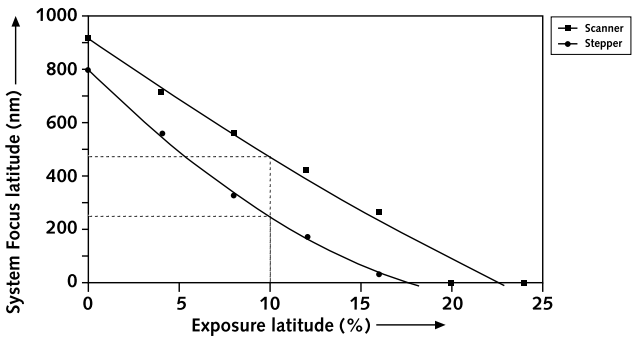

Figure 19b Comparative stepper / scanner system focus exposure window for 0.20 μm lines and spaces at 10% CD variation using a 0.63 NA DUV lens (data includes field and wafer flatness)

At 10% energy tolerance, the system depth of focus of the stepper (0.26 μm) is about 45% less than for the scanner (0.48 μm).

4. STEP-AND-REPEAT VERSUS STEP-AND-SCAN — EVALUATION

The factor of two improvement in the distortion, obtained when comparing full field distortion plots with simulated scanned distortion plots, is also expected in machine-to-machine distortion matching. However, this improvement is offset by stage synchronisation errors and stage grid distortion. Because the full field stepper distortion of current advanced wafer steppers is already below 40 nm, the 20 nm distortion advantage will be nearly eliminated by the additional grid matching and stage synchronisation. As shown, the stage synchronisation is about 5 nm. The stage matching is expected to be in the order of 15 nm. In general, the single machine overlay will be marginally worse and the machine-to-machine overlay will be marginally better, by several nanometers.

Clearly, there is an advantage in imaging performance using scanners instead of steppers. This advantage increases significantly when reducing the feature size. At 0.25 μm resolution, the process latitude advantage needs to be balanced with the cost disadvantage. The outcome of this balance depends, of course, on the application but we believe that DUV steppers will give more than adequate process latitude for most applications at 0.25 μm resolution. Only large field size requirements, above 22 x 22 mm, will force users to accept the higher cost and use scanners. However, if the resolution shrinks to 0.20 μm, we see the difference between scanner and stepper process latitude increase by a factor of two, forcing the balance in the direction of scanners, independent of the field size requirements. The economic balance between steppers and scanners, however, depends highly on the scanner system design. Compared to steppers, the additional scanner production capacity cost of 27%, calculated here, can easily exceed 50% if slow stage speed, low energy doses, high laser power and inaccurate dose control technologies are used.

In general, the above imaging and overlay advantages are reduced by additional error sources not taken in to account in the above analysis. Major error sources, not uniquely related to steppers or scanners, are reticle CD, reticle overlay variation, the process influence on CD variation and the process influence on overlay errors. These errors, which are assumed to apply equally to steppers and scanners, will reduce the imaging difference in a real production environment.

5. NEW DUV STEPPER PERFORMANCE

5.1. System description

Figure 20 shows the system layout of the PAS 5500/300 DUV wafer stepper with a numerical aperture variable from 0.40 to 0.57.

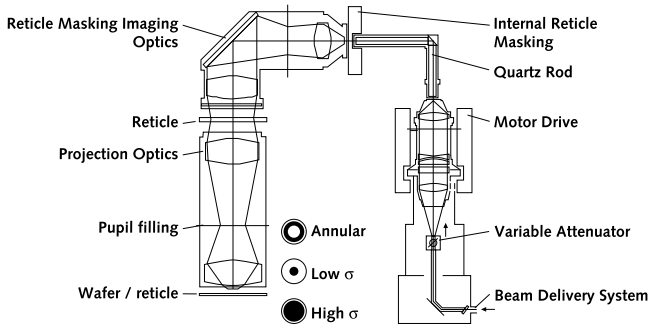

Figure 20 System overview of the PAS 5500/300 DUV wafer stepper, 22 x 22 mm, 0.40 ~ 0.57 NA

The field size is 22 x 22 mm and can be matched to its i-line counterpart, the PAS 5500/200 [12] with the same field size. The lens is double telecentric to reduce reticle unflatness effects in the distortion pattern. The magnification is four times, selected for reticle compatibility with future step-and-scan products. Lens (set) elements are servo-adjustable to correct magnification, third order distortion and field curvature.

Furthermore, the system contains a new AERIAL™ illumination system that is compatible with the recently published i-line counterpart, the PAS 5500/200 [12]. This system allows users to modify the job-controlled coherence value from 0.35 to 0.8. Also, job-controlled annular illumination modes can be used. The outer ring width can be varied from 0.35 to 0.8 and the inner ring width from 0.1 to 0.5, with a ring minimum of 0.3. Pupil shaping can be varied with a minimum impact on the illumination power and lens aberration at the wafer plane. The intensity stays within ±10% and the distortion within 35 nm. The system contains a reticle masking system which is imaged on to the reticle plane to maximize the reticle area utilization. The system can be equipped with lasers from various laser suppliers. The data shown here were taken with the CYMER 4600 laser at a frequency of 600 Hz, 6 W at 0.8 pm band width.

The new system is capable of exposing 80 eight inch wafers per hour at 30 mJ/cm^2 using a laser at 1000 Hz and 10 W illumination power resulting in a wafer level intensity of 225 mW/cm^2. The system is capable of exposing with a single machine overlay of 45 nm.

5.2. Lens performance, distortion and field flatness

The distortion of the new DUV lens is shown in Figure 21a, which is measured with the system's alignment system. The measured distortion is corrected for correctable distortion components [9].

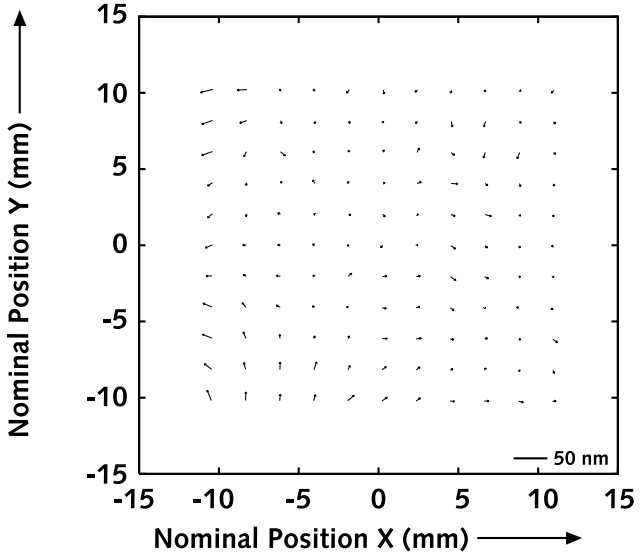

Figure 21a Distortion of the a 22 x 22 mm, DUV lens, σ = 0.75, NA = 0.57, max < 23 nm

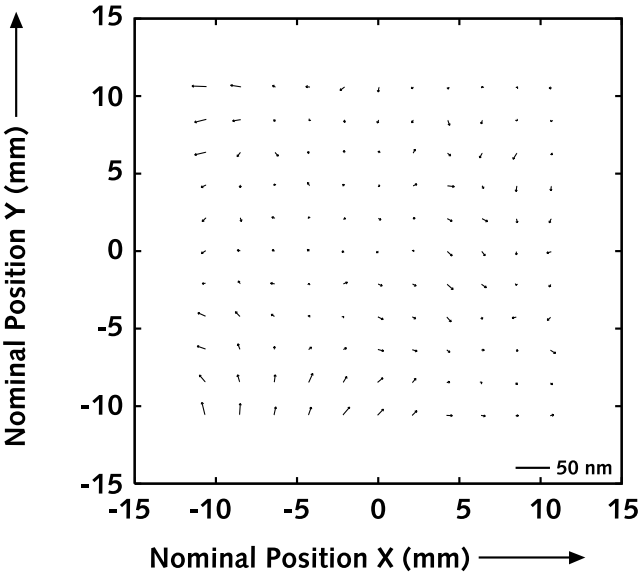

Figure 21b Distortion of the a 22 x 22 mm, DUV lens, σ_i= 0.45, σ_o = 0.75, NA = 0.54, max < 24 nm

Figure 21a is taken at a coherence (σ) of 0.75 and an NA of 0.57, Figure 21b shows the distortion plot measurements taken with an annular illumination at a

coherence (σ) of 0.45/0.75 at the inner/outer ring and a numerical aperture of 0.54.

The maximum distortion, measured in both numerical apertures and illumination modes, is smaller than 24 nm and shows negligible dependence on numerical aperture and illumination mode variation. Figure 22a shows the field flatness measured with the stepper alignment system [10].

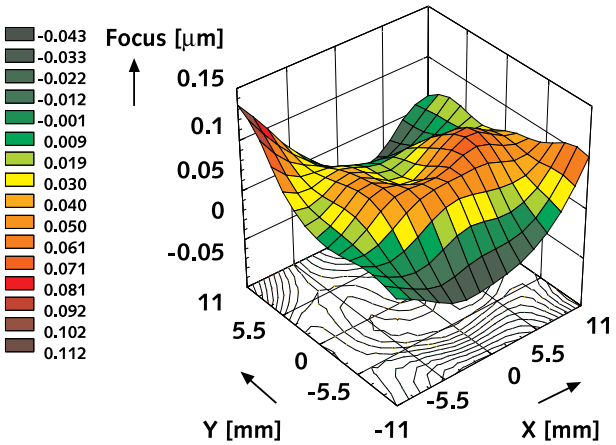

Figure 22a Field flatness of the 22 x 22 mm, DUV lens. Average focus position of horizontal and vertical lines and spaces, σ = 0.75, NA = 0.57, maximum range < 0,14 µm

Figure 22a shows the field flatness measured at a coherence (σ) of 0.75 and an NA of 0.57. Figure 22b shows the measurement taken at an annular illumination of 0.45/0.75 of the inner/outer ring and a numerical aperture of 0.54.

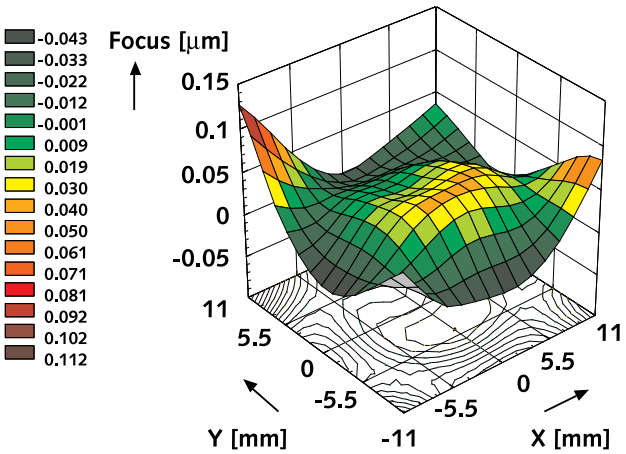

Figure 22b Field flatness of the 22 x 22 mm, DUV lens. Average focus position of horizontal and vertical lines and spaces, σ_t = 0.45, σ_o = 0.75, NA = 0.54, maximum range < 0.17 µm

Also, the field flatness data is corrected for correctable field flatness components. As shown for both numerical apertures and illumination settings, the field flatness remains below 0.17 µm and shows negligible dependence on numerical aperture and illumination variation.

5.3. Imaging performance

The PAS 5500/300 imaging is performed using 0.64 µm thick APEX-E-2408 resist processed using an FSI Polaris wafer track. Figure 23 shows the depth of focus of 0.25 to 0.175 µm lines and spaces at selected apertures and exposure dose.

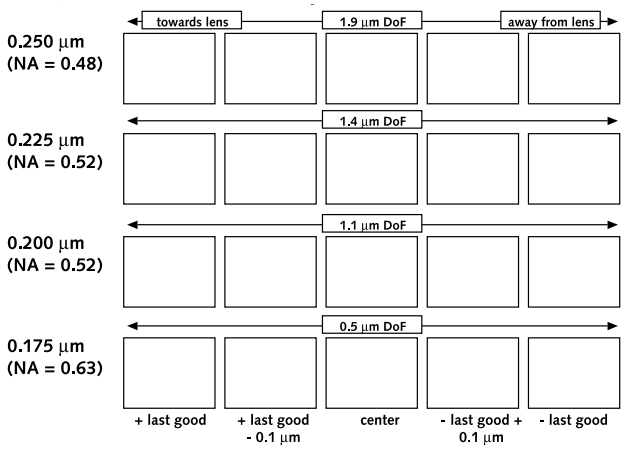

Figure 23 Depth of focus of 0.25, 0.225, 0.20 and 0.175 µm lines and spaces of a 22 x 22 mm, 0.57 NA DUV lens at optimum NA, σ_o = 0.75, σ_t = 0.45, 0.64 µm APEX-E-2408

The illumination mode used is annular, with an outer ring of 0.75 and an inner ring of 0.45. This illumination mode is used for all resist evaluations shown in this section. As shown, the depth of focus is 1.9 µm, at 0.25 µm lines and spaces, and reduces to 0.5 µm, at 0.175 µm lines and spaces.

At a numerical aperture of 0.48, the linearity is as shown in Figure 24.

Good linearity is shown from 0.425 µm to 0.225 µm lines and spaces. At these fine resolutions, it was difficult to separate reticle CD variation from process CD variation.

Figure 25 shows the focus exposure latitude at the same numerical aperture and illuminator settings as used to expose the 0.25 µm lines and spaces of Figure 23.

A depth of focus of 1.7 µm is measured, tolerating a 10% CD variation and 10% exposure variation. Further work is needed to evaluate the different numerical

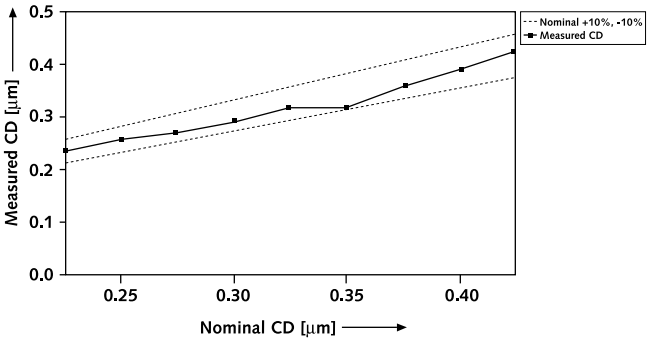

Figure 24 Linearity, nominal versus resist resolution, NA = 0.48, σ_o = 0.75, σ_i = 0.45, 0.64 μm APEX-E-2408

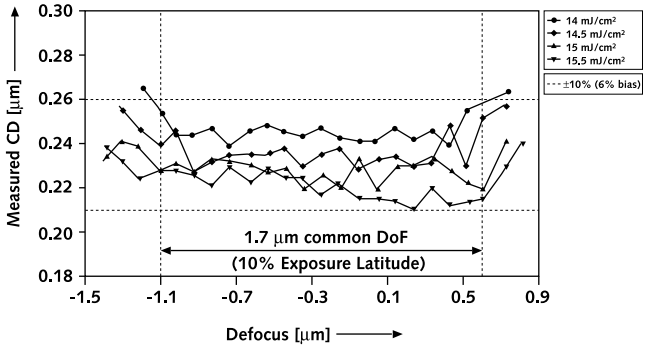

Figure 25 Focus exposure window for 0.25 μm lines and spaces at 10% CD variation, 6% bias, NA = 0.48, σ_o = 0.75, σ_i = 0.45, 0.64 μm APEX-E-2408

aperture and illumination settings as well as structure dependency, such as contacts and isolated lines. However, it is clearly shown that sufficient process latitude is shown for using DUV steppers at 0.25 μm design rules.

6. CONCLUSIONS

6.1. Stepper and scanner comparison

At 0.25 μm, it is expected that steppers, with a field size of 22 x 22 mm matching the existing installed i-line base, will be an optimum solution for cost effective manufacturing. As field size needs to increase and resolution needs to progress beyond 0.25 μm, scanners will play an increasingly central role, where scanning advantages in overlay improvements and process latitude extension begin to be of importance. Factors contributing to this conclusion are:

- Step-and-repeat systems have a fundamental exposure time advantage compared to step-and-scan systems where the reticle needs to be scanned in and out of the exposure field. Furthermore, the maximum stage scan speed will put a lower limit on the exposure time at low energy doses.
- Scanning can reduce dynamic lens distortion to 50%, dynamic field flatness to 75% and dynamic wafer flatness to 60% of the full field static values.
- Pulsed laser sources, used on DUV scanners, have the disadvantage that, to achieve sufficient intra-die exposure dose uniformity, the pulse to pulse variation divided by the laser frequency will set a limit on the minimum exposure time.
- Mercury lamp scanners (at i-line or DUV) have the additional disadvantage that a small exposure slit field will limit the optical power on the wafer and so limit the minimum exposure time.
- System depth of focus is introduced to describe the available process latitude and wafer-level CD variation. The system depth of focus using step-and-scan at 10% energy and CD tolerance is about 27% more than step-and-repeat systems with 0.25 μm lines and spaces. This number is about 45% for 0.20 μm lines and spaces.
- Though i-line scanners have an economic disadvantage compared to the optimum i-line stepper design, cost effective device manufacturing with DUV scanners will require mix-and-match with i-line scanners of compatible field sizes.

6.2. Step-and-scan technology

For scanner developments in general the following conclusions are drawn:

- Both stage technology and the parameters determining the slit width need to be matched and will mainly determine the economic competitiveness of step-and-scan systems. For DUV, the slit width is coupled to the dose control technology. For i-line, the slit width is coupled to the required illumination power to match the maximum scan speed.
- Stage synchronization can be achieved at > 200 mm/s with 5 nm accuracy, compatible with 0.18 μm lithography. At this resolution, 3% contrast loss has to be taken in to account when averaging over an 8 mm slit.
- It is expected that a 248 nm scanner will be capable fo being used at 0.18 μm by taking advantage of the improved CD behaviour in combination with advanced illumination techniques.

6.3. Steppers at 0.25 μm imaging

For the use of DUV steppers at 0.25 μm imaging, the following conclusions can be drawn:

- DUV lenses with a variable 0.40 ~ 0.57 NA can be built showing 25 nm distortion and 0.2 μm flatness delivering more than 1 μm depth of focus necessary to

reliably produce 0.25 μm lines and spaces.

- Imaging performance extensions can be expected using fully automated, production compatible, variable coherence, annularity and numerical aperture. Furthermore, four image parameters including magnification, distortion and field curvature can be continuously optimized.

APPENDIX 1. SOURCE BRIGHTNESS, OPTICAL THROUGHPUT AND LIGHT INTENSITY

The brightness of an illumination source can be defined by [13]:

$$dP = B(x, y, \alpha, \beta) \cdot \cos\theta \cdot dA \cdot d\Omega \qquad \text{(A.1.1)}$$

Where:

dP	: Total illumination power illuminated from a surface dA and cone $d\Omega$ from a source with brightness B	[W]
B	: Source brightness at a surface element located at coordinate x, y in the direction α, β	[W/mm^2.Sr]
θ	: Angle between the source brightness and surface normal	[rad]
dA	: Radiating surface	[mm^2]
$d\Omega$	: Radiating solid angle	[Sr]

If B is constant over a surface A and a solid angle cone Ω is centred perpendicularly to the surface (see Figure 26), we see:

$$P = B \cdot A \cdot \Omega \qquad \text{(A.1.2)}$$

For the purpose of this article, we will use the above simple expression of brightness. This is useful for the scope of this article but will limit the validity of the conclusions to about 20 or30% depending on the source geometry.

The ability of an optical system to transmit energy is determined by a combination of the sizes of the field stop and the pupil in the same optical space. This ability can be called optical throughput or entendue and can be written as [14]:

$$E = A \cdot \Omega \qquad \text{(A.1.3)}$$

This reduces (A.1.2) to:

$$P = B \cdot E \qquad \text{(A.1.4)}$$

Figure 26 is the layout of a typical mercury lamp source.

Since the plasma energy density is limited to a maximum value due to the limited plasma temperature guaranteeing an acceptable lamp life time, all state of the art photolithography lamps have about the same optical brightness. Assuming the plasma size fills up the space between the electrodes, the mercury lamp throughput is equal to:

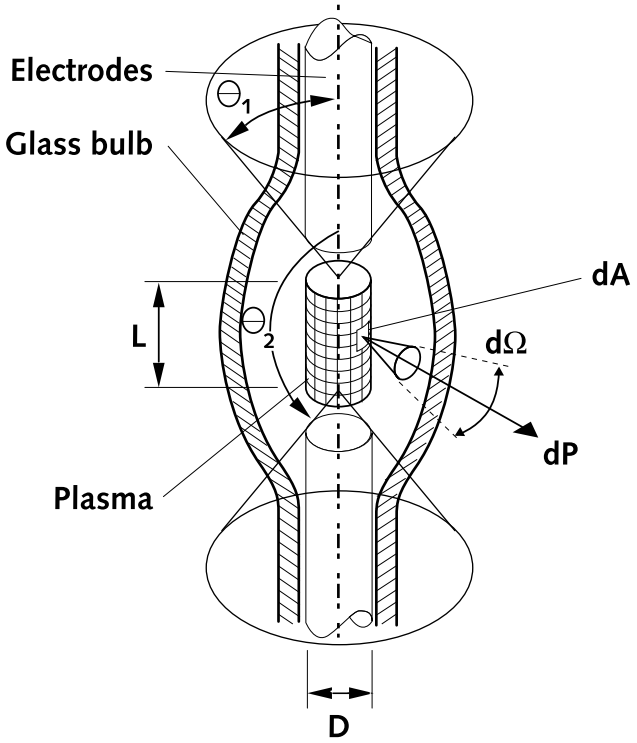

Figure 26 Mercury lamp bulb

$$E_s = 2 \cdot \pi^2 \cdot D \cdot L \cdot (\cos\theta_1 - \cos\theta_2) \qquad \text{(A.1.5)}$$

Where:

E_s	: Source throughput	[W/mm^2.Sr]
D	: Electrode diameter	[mm]
L	: Electrode spacing	[mm]
θ_1, θ_2	: Radiation angle	[rad]

We can check the constant brightness assumption, as shown in Figure 27.

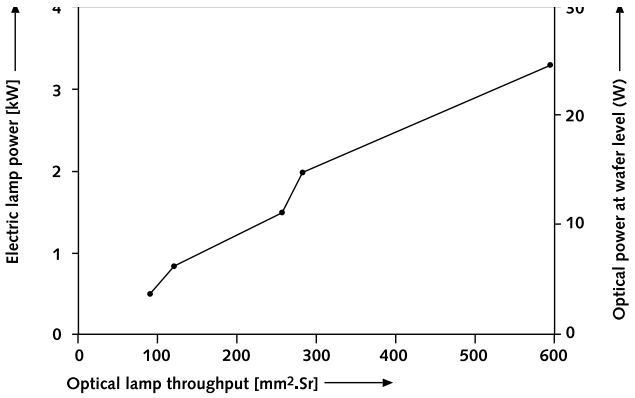

Figure 27 Electrical/optical mercury lamp power as function of optical throughput

The electrical power of different mercury lamps is shown as function of the calculated throughput according to (A.1.5). For the different lamp types shown, the electrical to optical efficiency is constant; this enables the use of the two scales in the figure simultaneously. The linearity between lamp power and lamp throughput as a result of the constant brightness is clearly visible.

Applying the above theory to the wafer stepper optics containing a light source, in-couple optics, illuminator optics and projection optics, such as shown in Figure 28, we can define four different optical throughput values of those separated optical systems, E_s, E_i, E_r and E_w.

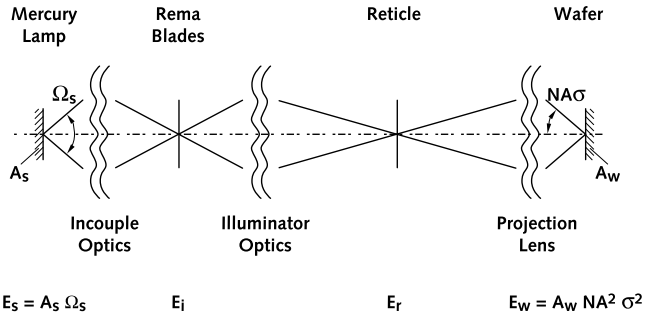

Figure 28 Optical system of a wafer stepper, from source to wafer

The effective optical throughput of the total system is now given by:

$$E_{eff} = min(E_s, E_i, E_r, E_w) \qquad \text{(A.1.6)}$$

In a practical system, the in-couple optics determine the effective optical throughput of the system. The in-couple optics need to adapt the lamp throughput shape to the lens throughput shape by using kaleidoscopes, fly's eye integrators, phase plates etc. The quality of the in-couple optics is determined by how closely the effective system throughput can match the lamp throughput without energy loss. The lamp throughput needs to be selected to be slightly larger than that of the in-couple optics. A larger lamp throughput will increase the electrical and optical lamp power and corresponding heat dissipation without increasing the transmitted power. Also, the lens throughput will be selected such that the effective source will slightly underfill the optics to achieve a coherence value lower than 1. Compared to the source, this leads to a higher lens throughput. Finally, the illuminator throughput will be designed such that the total captured illumination power will be transmitted to the wafer without using unnecessarily large and expensive optics.

This allows us to calculate that the amount of power, at wafer level, of a source with brightness *B* and an imaging system with transmission efficiency *e* is:

$$P_w = e \cdot B \cdot E_{eff} = e \cdot B \cdot E_i, \quad E_s > E_i \qquad \text{(A.1.7)}$$

Since the three-dimensional Helmholtz-Lagrange invariant of optical imaging [14] can be written as:

$$E = constant \qquad \text{(A.1.8)}$$

We can write (A.1.7) in terms of the wafer plane variables in the following approximation for values of the numerical aperture and coherence product being much smaller than one:

$$I_w = \pi \cdot e \cdot B \cdot NA^2 \cdot \sigma^2, \quad E_s > E_i \qquad \text{(A.1.9a)}$$

Where:

I_w	: Intensity at wafer level	[W/m^2]
e	: Optical transmission efficiency	
NA	: Numerical aperture of the projection lens	
σ	: Partial coherence	
E_s	: Source throughput	[m^2.Sr]
E_i	: Illuminator throughput	[m^2.Sr]

Equation (A.1.9a) is checked with an optical tracing program, where the optical power at wafer level is calculated by varying the slit width at various coherence values using a 2.5 kW lamp, as shown in Figure 29. The slit height is 26 mm and the numerical aperture is 0.6.

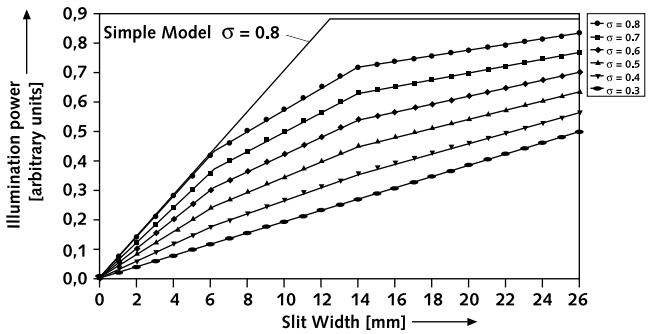

Figure 29 Relative power, at wafer level, a 2.5 kW mercury lamp in a, 0.6 NA, 31.1 mm round i-line system as a function of slit width at various coherence values

For low coherence values, the source throughput is much larger than the illuminator throughput and equation (A.1.9a) holds true. For large coherence values, however, the source throughput becomes, at a certain slit width, smaller than the illuminator throughput and the illumination power becomes less sensitive for slit width variations. In this graph, we see that the simplified model predicts a matched source and illuminator throughput at a slit diameter of 13 mm and a coherence value of 0.8, corresponding to a throughput of 245 mm^2.Sr. According to Figure 27, the throughput of a 2.5 kW lamp is 280 mm^2.Sr. As clearly shown in the area of matched throughput of the source and the illuminator, errors of up

to 20-30% of the simplified model have to be taken in to account.

For a laser source, the source brightness is extremely high and the source throughput is extremely low compared to mercury lamp sources. If the laser has a beam size of 20 x 5 mm with a divergency of 12 x 3 mrad, the throughput is about 10^{-2} mm^2.Sr, more that four orders of magnitude smaller than the mercury lamp throughput. In this case, the effective throughput is limited by the source for all practical system numerical apertures and field sizes. The intensity at wafer level is now simply given by:

$$I_w = e \cdot \frac{P}{A_w}, \qquad E_s < E_i \qquad \text{(A.1.9b)}$$

Where:

P	: Total optical source power	[W]
A_w	: Total illuminated wafer area	[m^2]

APPENDIX 2. STEP-AND-SCAN VERSUS STEP-AND-REPEAT EXPOSURE TIME

The step-and-repeat exposure time can be given by:

$$T_{sr} = \frac{D}{I_{sr}} \qquad \text{(A.2.1)}$$

Where:

T_{sr}	: The step-and-repeat exposure time	[s]
D	: Resist sensitivity, dose	[mJ/cm^2]
I_{sr}	: Step-and-repeat light intensity at wafer level	[mW/cm^2]

For a step-and-scan system, the exposure time is given by:

$$T_{ss} = \frac{W + S}{V} \qquad \text{(A.2.2)}$$

Where:

T_{ss}	: Step-and-scan exposure time	[s]
W	: Die width	[mm]
S	: Slit with at wafer level	[mm]
V	: Wafer scan speed	[mm/s]

The scan speed of the scanner is given by:

$$V = \frac{I_{ss} \cdot S}{D} \qquad \text{(A.2.3)}$$

Where:

I_{ss}	: Step-and-scan light intensity at wafer level	[mW/cm^2]

Consider, now, step-and-scan systems and step-and-repeat systems of equal capability. By exposing a die of width, W, and height, H, with the same resolution (same NA and σ), we have the following relationships for the intensity of the step-and-scan and step-and-repeat systems (see Appendix 1):

$$I_{ss} \cdot S = I_{sr} \cdot W, \qquad \text{for } E_s < E_{ss} \qquad \text{(A.2.4a)}$$

$$I_{ss} = I_{sr}, \qquad \text{for } E_s > E_{sr} \qquad \text{(A.2.4b)}$$

$$(I_{ss} \cdot S \cdot E_s = I_{sr} \cdot W \cdot E_{ss}, \qquad \text{for } E_{ss} < E_s < E_{sr}) \qquad \text{(A.2.4c)}$$

Where:

E_s	: Source throughput	[m^2.Sr]
E_{ss}	: Step-and-scan throughput	[m^2.Sr]
E_{sr}	: Step-and-repeat throughput	[m^2.Sr]

Note: We assume that $S < W$ so that $E_{ss} < E_{sr}$.

Equations (A.2.4a) and (A.2.4b) include the extreme cases $E_s \gg E_{sr}$ and $E_s \ll E_{ss}$ where the equations hold true even for sources that do not have sharply defined throughputs. In particular, equation (A.2.4c) has, for this reason, limited validity.

Now, from (A.2.1), (A.2.2), (A.2.3), (A.2.4a), (A.2.4b) and (A.2.4c), we can write down the comparable step-and-scan and step-and-repeat exposure times:

$$T_{ss} = T_{sr} \cdot \left(1 + \frac{S}{W}\right), \qquad \text{for } E_s \ll E_{ss} \qquad \text{(A.2.5a)}$$

and

$$T_{ss} = T_{sr} \cdot \left(1 + \frac{W}{S}\right), \qquad \text{for } E_s \gg E_{sr} \qquad \text{(A.2.5b)}$$

This equation means that, for a high brightness source, the slit width can be minimised to minimise the exposure time, which goes hand-in-hand with minimizing lens cost. For a low brightness lamp, such as a large power mercury i-line lamp, the slit width needs to be maximized, leading to a larger difference from step-and-repeat exposure times with no lens cost advantage.

APPENDIX 3. PULSED ILLUMINATION SOURCE SCANNER EXPOSURE TIME

The wafer intensity of a DUV scanner can, according to (A.1.9b), be given by:

$$I_{ss} = \frac{e \cdot P_p \cdot f}{H \cdot S} \qquad \text{(A.3.1)}$$

Where:

I_{ss} : Step-and-scan intensity at wafer level [W/cm^2]
e : System efficiency
P_p : Source pulse power [J]
H : Illumination height at wafer level [cm]
S : Illumination slit at wafer level [cm]
f : Pulse frequency [Hz]

Since a minimum n pulses is needed to make a dose with the required dose accuracy, relationship (A.2.3) is bounded by the following maximum wafer speed to achieve sufficient dose control:

$$V < S \cdot \frac{f}{n} \qquad \text{(A.3.2)}$$

Where:

V : Wafer scan speed [mm/s]
n : Minimum number of pulses to make energy dose accurately

Since the stage technology determines the maximum scan speed that can be used, it makes sense to match the stage technology limitation and the dose control technology limitation by:

$$S = V_m \cdot \frac{n}{f} \qquad \text{(A.3.3)}$$

Where:

V_m : Maximum wafer scan speed [mm/s]

Combining (A.3.1), (A.3.3), (A.2.2) and (A.2.3) results in the following exposure time for pulsed laser sources on scanners:

$$T_{ss} = \left(\frac{V_m}{V}\right) \cdot \left(\frac{W}{V_m} + \frac{n}{f}\right) \qquad \text{(A.3.4a)}$$

with:

$$V = A \cdot \frac{e \cdot P_p \cdot f}{H \cdot D} \qquad \text{(A.3.4b)}$$

and:

$$A = \frac{V_m \cdot H \cdot D}{e \cdot P_p \cdot f} < 1 \qquad \text{(A.3.4c)}$$

Where

T_{ss} : Step-and-scan exposure times [s]
A : Laser attenuator

The minimum number of pulses required to achieve an accurate dose varies linearly with the pulse to pulse power variation of the laser:

$$n = D_k \cdot \Delta \qquad \text{(A.3.5)}$$

Where:

n : Minimum number of pulses to achieve the required illumination dose accuracy
Δ : Relative pulse to pulse power variation of the laser
D_k : Linearity factor determined by the dose control technology of the laser and stepper [7]

From equations (A.3.4a), (A.3.4b) and (A.3.4c), we see that the scanner throughput is strongly connected to the following laser parameters:

1. Maximise laser power to $P_p.f$. The pulse power can only be increased while the laser frequency is high enough to prevent the attenuator, defined in equation (A.3.4c), departing from 1.
2. Minimise the overscan time by minimizing $\Delta / P_p.f^2$. High laser frequency is only advantageous if, at most, only a moderate decrease of pulse-to-pulse power variation and pulse power is taking place.

The limitation of the minimum number of pulses, n, also exists on steppers but is less critical. The minimum dose not requiring laser attenuation for a scanner is different for a stepper and holds the following relation, assuming the same illumination height, and the same D_k factor on the stepper and on the scanner:

$$D_{ssmin} \cdot W = D_{srmin} \cdot S \qquad \text{(A.3.6)}$$

Where:

D_{ssmin} : Minimum dose in the scanner [J/cm^2]
D_{srmin} : Minimum dose in a stepper [J/cm^2]
W : Illumination width on the stepper [cm]
S : Slit width on the scanner [cm]

Since $S < W$, the minimum dose with effective throughput on a stepper is always lower than on a scanner.

APPENDIX 4. COST OF I-LINE SCANNING

For laser scanning, as used in 248 nm lithography, the economics of scanning is easy; the scanning slit and the lens field size need to be as small as the dose control requirements allow. For non-laser scanning, the situation is more complex. For a small scan slit system, the amount of light through the lens is minimal, leading to long exposure time. If the slit is enlarged, the field size increases together with the amount of light and the throughput while, at the same time, the system cost increases. With the help of a simplified model, we can show this mechanism.

The system cost consists of the basic body cost, B, the optics cost, L, and the additional scanning stage cost, SC.

The wafer time consists of the exposure time, *T*, the step time, *ST*, and the overhead time, *O*. As an economic indicator, we can now calculate the required investment, or system cost, per unit production capacity, or system throughput in wafers per second:

$$PCC_{ss} = (B + SC + L) \cdot (T + ST + O) \qquad \text{(A.4.1)}$$

Where:

PCC_{ss}	: Production capacity cost of a step-and-scan system	[$.s/wafer]
B	: Body cost	[$]
SC	: Additional scanner cost compared to a stepper	[$]
L	: Lens cost	[$]
T	: Total wafer expose time	[s/wafer]
ST	: Total step time per wafer	[s/wafer]
O	: Overhead time per wafer	[s/wafer]

According to Figure 1, the lens cost can be described by:

$$L = K \cdot (H^2 + S^2) \qquad \text{(A.4.2)}$$

Where:

K	: Lens cost per unit exposure field	[$/mm^2]
H	: Die height	[mm]
S	: Slit width	[mm]

Assuming that mercury lamp technology has no power limit, we can assume that the source throughput is always larger than the system throughput or $E_S \gg E_{sr}$, as discussed in Appendix 1. In this case, the intensity of scanners is constant and independent of the exposure field.

Combining these two equations and including (A.2.5b), we get, for scanners, the following economic system throughput:

$$PCC_{ss} = (B + SC + K \cdot (H^2 + S^2)) \cdot \left(T_{sr} \cdot \left(1 + \frac{W}{S}\right) + ST + O\right) \qquad \text{(A.4.3a)}$$

Where:

T_{sr}	: Total step-and-repeat exposure time per wafer	[s/wafer]

For the step-and-repeat version, we can remove the W/S term, replace S by W and leave the additional scanner hardware cost, to give the following production capacity cost for steppers:

$$PCC_{sr} = (B + K \cdot (H^2 + W^2)) \cdot (T_{sr} + ST + O) \qquad \text{(A.4.3b)}$$

For small slit width, the capacity cost increases because of a dramatic increase of the exposure time. For large slit width, the capacity cost increases because of the large lens cost. A compromise between lens cost and exposure time needs to be made.

For scanners, there is an advantage because the increase of the die width will not lead to an increase of the lens cost.

The additional scanner hardware cost and the increased exposure time for i-line scanners will almost completely offset the reduced lens cost. The economic comparison between i-line scanners and steppers can be significantly worse for scanners depending upon the details of the illumination system and mercury lamp design.

APPENDIX 5. THE CD MODEL

This appendix discusses a method for comparing critical dimension (CD) performance of steppers and scanners. For CD analysis of stepping systems, there is a wide variety of simulation packages available (for example, Prolith 2, Solid-C etc.). With these packages, the CD performance of an exposure tool, including the required processing, can be simulated. For scanning systems, no simulation packages are yet widely available. The imaging part of the model has to be modified. In a stepping system, the image is calculated for one particular focus height while, in a scanning system, the image is built up from multiple exposures at various focus heights (*Z*) and at varying positions *(X, Y)*. Taking these effect into account with current simulation software would be very time consuming. For this reason, we have selected a simple approach based upon the aerial image. The aerial image of a scanning system is calculated by superposition of the individual exposures.

The CD simulation in this paper is based upon the aerial image simulation of dense line and space structures. The image is calculated with the Prolith simulation program [15] and is a function of lens and image set-up parameters. Lens parameters are the resolution, the numerical aperture, the coherence and the wavelength of the projection system. The image set-up parameters are those parameters that have an impact on the actual focus height, the position of the image and the dose. Examples of these parameters are wafer non-flatness, focal plane deviation and *Z*-errors caused by metrology, levelling accuracy and XY errors.

The image of a stepping system is calculated for one focus position. It is assumed that the focus height and position variation during the exposure can be neglected. In a scanning system, the image is the sum of a number of individual exposures with different X, *Y* and *Z* positions.

Stepper image:

$$I(X, Y, Z(X, Y)) \qquad \text{(A.5.1)}$$

Scanner image:

$$I(X, Z(X)) = \frac{1}{S} \cdot \int_{\frac{-S}{2}}^{\frac{S}{2}} I(X, Y, Z(X, Y))dY \qquad \text{(A.5.2)}$$

Where:

I(X,Y,Z)	: Intensity of the aerial image	[mJ/cm^2]
X	: Image position in the non-scanning direction	[m]
Y	: Image position in the scanning direction	[m]
Z(X,Y)	: Focus position at location X.Y in the image	[m]
S	: Slit width	[m]

It is Important to realise that the imaging characteristics of the integrated image, described in (A.5.2), do not have any dependency on the coordinate in the scanned direction, *Y*. This is also visible in the distortion plot given in Figure 14b. A further consequence is that all uneven distortion terms in the scanned direction are eliminated. Examples of these terms are rotation, trapezoid, third and fifth order distortion in the scanned direction and wedge in the non-scanned direction.

The aerial image, calculated in (A.5.2), now needs to be translated into a line width calculation, including the dependence on dose, to be able to construct a focus exposure window. A practical approach is to define the CD width as the aerial image width at a certain intensity. This intensity is chosen nominally at nodal points in the aerial image. In this way, it is chosen around the iso-focal exposure dose:

$$I(X, Z) = I_0 \Rightarrow (X_1(Z, I_0), X_2(Z, I_0)) \qquad \text{(A.5.3a)}$$

$$CD(Z, I_0) = |X_1 - X_2| \qquad \text{(A.5.3b)}$$

Where:

I_0	: Intensity level for which the CD is calculated,	[mJ/cm^2]
X_1,X_2	: Solution of the contrast threshold equation	[m]

The equations (A.5.1), (A.5.2), (A.5.3a) and (A.5.3b) are now solved *n* times, where the image set-up parameters *X, Z* and I_0 are varied with a random error simulator according to Table 2. The error sources for the model input parameters have a normal distribution. As a result, *n* CD values are calculated, both for stepper operation, using the stepper error distribution, and for scanner operation, using the scanner error distribution.

The numerical translations for (A.5.1), (A.5.2), (A.5.3a) and (A.5.3b) are:

$$I_j(X, Z) = \frac{1}{j} \cdot \sum_{i=1}^{j} I_i((X + dX_i), (Z + dZ_i)) \qquad \text{(A.5.4a)}$$

$$I_j(X, Z) = I_0 + dI_{0j} \Rightarrow (X_{1j}(Z, I_0), X_{2j}(Z, I_0)) \qquad \text{(A.5.4b)}$$

$$CD_j(Z, I_0) = |X_{1j} - X_{2j}| \qquad \text{(A.5.4c)}$$

Where:

dX	: Position noise	[µm]
dZ	: Focus noise	[µm]
dI_0	: Dose noise	[µm]

The CD distribution can be used for the construction of the ED window. The CD simulator gives the extreme CD values as a function of the exposure and focus offset, the extreme vales may not exceed the 10% criterion of the nominal CD value. The extreme CD values are defined as follows:

$$CD_{max} = CD_{mean}(Z, I_0) + 3 \cdot CD_{\sigma}(Z, I_0) < 1.1 \cdot CD_{nom} \qquad \text{(A.5.5a)}$$

$$CD_{min} = CD_{mean}(Z, I_0) - (3 \cdot CD_{\sigma}(Z, I_0)) > 0.9 \cdot CD_{non} \qquad \text{(A.5.5b)}$$

Where:

CD_{nom}	: Nominal CD value	[µm]
CD_{max}	: Maximum CD value	[µm]
CD_{min}	: Minimum CD value	[µm]
CD_{mean}	: Mean CD value	[µm]
CD_{σ}	: Standard deviation of the CD values	[µm]

The statistical variables are determined from the CD_j values, as shown in equations (A.5.4a), (A.5.4b) and (A.5.4c).

Figure 30a gives the simulated results for a DUV stepper printing 250 nm resolution.

Figure 30b gives the same results for a scanning system.

As shown the difference between steppers and scanners are small for small focus and exposure errors. For larger focus and exposure offsets the CD variation of the scanner system is smaller that the stepper system.

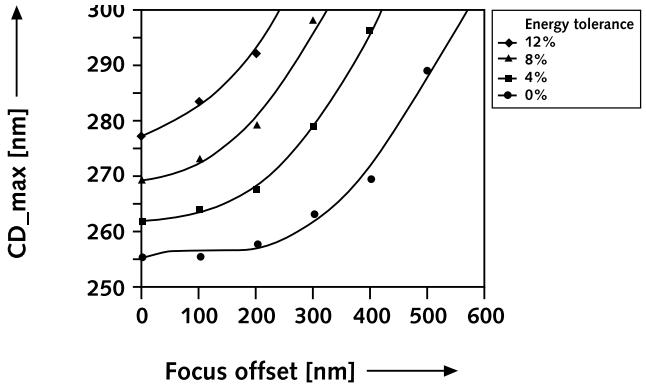

Figure 30a Maximum CD versus focus offset at various energy dose tolerances imaging 0.25 μm lines and spaces, NA = 0.6, σ = 0.7, DUV Stepper mode

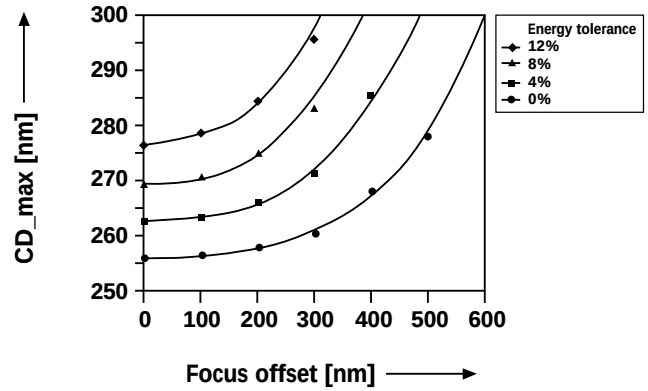

Figure 30b Maximum CD versus focus offset at various energy dose tolerances imaging 0.25 μm lines and spaces, NA = 0.6, σ = 0.7, DUV Scanner mode

ACKNOWLEDGMENTS

The analysis in this paper and, in particular, the experimental data from the step-and-scan prototype have more contributors than there is space in the authors' list. In addition to the DUV project team at ASML, major contributions are incorporated from Philips centre for manufacturing technology, Philips research and Carl Zeiss.

REFERENCES

[1] "The National Technology Roadmap For Semiconductors", SIA Semiconductor Industry Association, preliminary version, published by J. Cannin at the advanced optics workshop, SEMATECH, Dallas, February 1996.

[2] S. Wittekoek, "Optical lithography: present status and continuation below 0.25 μm", Microelectronic Engineering 23, October1994, pp 43-55.

[3] H. Shimiza, "Production technology systems and process equipment", Technical proceedings SEMI technology symposium, Chiba, Japan, December 1994, pp115-125.

[4] D. A. Markle, "The future and potential of optical scanning systems", Solid State Technology, September 1984, pp 159-166.

[5] J. D. Buckley, C. Karatzas, "Step and scan, a systems overview of a new lithography tool", SPIE vol.1088, Optical/laser lithography II, San Jose, March 1989, pp424-433.

[6] S. Marakami, "Optical exposure system today and future", Technical proceedings SEMI technology symposium, Ciba, Japan, December 1994, pp 397-406.

[7] D. H. Tracy, F. Y. Wu, "Exposure dose control technique for excimer laser lithography", SPIE Vol. 922, Optical/laser lithography, Santa Clara, March 1988, pp437-443.

[8] H. Kawai, "Throughput of stepper for 300 mm wafer", Technical proceedings SEMI technology symposium, Chiba, Japan, December 1995.

[9] M. A. van den Brink, C. G. M. de Mol, R. A. George, "Matching performance for multiple wafer steppers using an advanced metrology procedure", SPIE vol.921, Integrated circuit metrology, inspection and process control II, Santa Clara, March 1988, p 180.

[10] P. Dirksen, "Latent image metrology for production of wafer steppers", SPIE Vol. 2440, Santa Clara, March 1995, pp 701-711.

[11] J. Bischhof, W. Henke, J. v. d. Werf, P. Dirksen, "Simulations on step & scan optical lithography, SPIE Vol 2197, San Jose, March 1994, p 953.

[12] J. Mulkens et al, "High throughput wafer steppers with automatically adjustable conventional and annular illumination modes, Proceedings technical seminar Semicon Japan, Ciba, December 1995, pp 3-30.

[13] M. Born, E. Wolf, Principles of optics, Pergamon Press, Oxford, 1980 (6), p 181.

[14] R. S. Longhurst, Geometrical and physical optics, Longman, Burnt Mill, 1973 (3), p 466.

[15] C. Mack, "Prolith: a comprehensive optical lithography model", SPIE, vol 530, Santa Clara, March 1985, pp 207-220.